Positional dynamics and glycosomal recruitment of developmental regulators during trypanosome differentiation

Balázs Szöőr [a#], Dorina V. Simon[a], Federico Rojas[a], Julie Young[a], Derrick R. Robinson[b], Timothy Krüger[c], Markus Engstler[c] and Keith R. Matthews[a#]

Running title: Trypanosome development

a. Institute for Immunology and Infection Research, School of Biological Sciences, University of Edinburgh; Edinburgh, EH9 3JT, United Kingdom
b. CNRS, Microbiology Fundamental and Pathogenicity, MFP UMR 5234, University of Bordeaux,146 rue Léo Saignat, Batiment 3A - 1er étage, 33076 Bordeaux Cedex; Bordeaux, France.
c. Cell and Developmental Biology; University of Würzburg; Biozentrum; Am Hubland; D-97074 Würzburg; Germany

5054 words

[#]Address correspondence to:

Balázs Szöőr; Balazs.Szoor@ed.ac.uk

Keith R Matthews; keith.matthews@ed.ac.uk

Abstract

Glycosomes are peroxisome-related organelles that compartmentalise the glycolytic enzymes in kinetoplastid parasites. These organelles are developmentally regulated in their number and composition, allowing metabolic adaptation to the parasite's needs in the blood of mammalian hosts or within their arthropod vector. A protein phosphatase cascade regulates differentiation between parasite developmental forms, comprising a tyrosine phosphatase, TbPTP1, that dephosphorylates and inhibits a serine threonine phosphatase TbPIP39 that promotes differentiation. When TbPTP1 is inactivated, TbPIP39 is activated and during differentiation becomes located in glycosomes. Here we have tracked TbPIP39 recruitment to glycosomes during differentiation from bloodstream stumpy forms to procyclic forms. Detailed microscopy and live cell imaging during the synchronous transition between life cycle stages revealed that in stumpy forms, TbPIP39 is located at a periflagellar pocket site closely associated with TbVAP, that defines the flagellar pocket endoplasmic reticulum. TbPTP1 is also located at the same site in stumpy forms, as is REG9.1, a regulator of stumpy-enriched mRNAs. This site provides a molecular node for the interaction between TbPTP1 and TbPIP39. Within 30 minutes of the initiation of differentiation TbPIP39 relocates to glycosomes whereas TbPTP1 disperses to the cytosol. Overall, the study identifies a 'stumpy regulatory nexus' (STuRN) that co-ordinates the molecular components of life cycle signalling and glycosomal development during transmission of *Trypanosoma brucei*.

Importance

African trypanosomes are parasites of sub-Saharan Africa responsible for both human and animal disease. The parasites are transmitted by tsetse flies and completion of their life cycle involves progression through several development steps. The initiation of differentiation between blood and tsetse forms is signalled by a phosphatase cascade, ultimately trafficked into peroxisome-related organelles called glycosomes that are unique to this group of organisms. Glycosomes undergo substantial remodelling of their composition and function during the differentiation step but how this is regulated is not understood. Here we identify a cytological site where the signalling molecules controlling differentiation converge before the dispersal of one of them into glycosomes. This coincides with a specialised ER site that may contribute to glycosome developmental biogenesis or regeneration. In combination, the study provides the first insight into the spatial co-ordination of signalling pathway components in trypanosomes as they undergo cell-type differentiation.

Introduction

The dynamic regulation of organelle biogenesis or composition often involves intimate contact between the endoplasmic reticulum and the membrane of the target organelle (1). This enables the maturation and modification of organellar protein content, influencing mitochondrial, Golgi or peroxisomal components, whereas inter-organellar contacts can also contribute to signalling events within cells, bringing regulatory molecules into proximity, or trafficking them for degradation (2). The protein contacts at the interface between organelles are often diverse and characteristic of each organellar type, predominantly interacting with vesicle associated membrane protein associated proteins (VAPs) on the ER membrane.

In addition to the conventional organelles typical of eukaryotic cells, evolutionarily divergent kinetoplastid parasites are characterised by their possession of glycosomes, specialist organelles that harbour the enzymes of glycolysis (3). Although unique in their compartmentation of glycolytic enzymes, glycosomes are related to peroxisomes, sharing with those organelles a similar (though divergent) machinery for import, insertion of membrane proteins (PEX16, PEX19) and peroxisome proliferation, as well as their capacity for either lipid, purine and pyrimidine biosynthesis (4). Glycosomes are also dynamic in composition and number in response to the metabolic demands of the parasite, their synthesis and turnover involving similar biogenesis and degradation mechanisms to those of the peroxisomes of yeast and mammalian cells. This capacity for biosynthesis and turnover enables peroxisomes and glycosomes to exploit different nutrient conditions or adapt to different developmental forms.

Kinetoplastid parasites comprise pathogens of mammals that are frequently transmitted by arthropod vectors. Among the best characterised and tractable are the African trypanosomes, *Trypanosoma brucei*. These parasites live extracellularly in the bloodstream

and tissues of mammalian hosts, where they cause human sleeping sickness and the livestock disease nagana (5, 6). Trypanosomes are spread by blood feeding tsetse flies, the passage between the blood and the insect gut involving a switch from glucose based energy metabolism to one reliant on amino acids (7). Pivotal to the successful colonisation of the tsetse fly are so called 'stumpy forms', quiescent bloodstream forms that show several adaptations for survival upon uptake by tsetse flies (8), including partial elaboration of their mitochondrion in preparation for the switch from glucose-dependent energy generation *via* glycolysis (9-12). Stumpy forms arise from proliferative slender forms in the bloodstream in a quorum sensing response dependent upon parasite density (13). This results in the accumulation of uniform populations of stumpy forms that are cell cycle arrested in G1/G0 and sensitised for differentiation when taken up in a tsetse fly blood meal (14), this culminating in the production of a population of differentiated procyclic forms that colonise the tsetse midgut. The same transition can also be enacted *in vitro* by exposing stumpy forms to reduced temperature and *cis*-aconitate/citrate, this generating a highly synchronised differentiation model allowing cytological events to be readily tracked and quantitated in the population (15).

The signalling events that stimulate the differentiation of stumpy forms to procyclic forms are quite well characterised. Thus, stumpy forms are held poised for differentiation by the action of a negative regulator of differentiation, TbPTP1, a tyrosine specific phosphatase (16, 17). A substrate of TbPTP1 is the DxDXT/V class serine threonine phosphatase TbPIP39, which is dephosphorylated on tyrosine 278 by TbPTP1, this interaction reducing the activity of TbPIP39 and so preventing differentiation (18). When exposed to reduced temperature, as would occur during a tsetse bloodmeal (19), blood citrate is transported by 'PAD' proteins whose expression is elevated on stumpy forms at 20ºC (20). When exposed to citrate/*cis*-aconitate, TbPTP1 is inactivated and TbPIP39 becomes phosphorylated and

activated, this stimulating differentiation of the parasites. Interestingly, sequence analysis of TbPIP39 revealed the presence of a PTS1 glycosomal localisation motif (-SRL) and this localisation was confirmed in procyclic forms by both its co-localisation with glycosomal markers (17) and its detection in glycosomal proteome analysis (21). This linked differentiation signalling in the bloodstream form parasites with glycosomal signalling during differentiation, with TbPIP39 being expressed in stumpy forms but not slender forms and being localised in glycosomes in procyclic forms.

Here we have exploited the differential expression and glycosomal location of TbPIP39 to explore the spatial positioning of differentiation signalling molecules during the transformation of stumpy forms to procyclic forms. Our results reveal the coincidence of TbPIP39 and TbPTP1 in bloodstream stumpy forms at a novel periflagellar pocket location, closely associated with a flagellar pocket ER contact site defined by TbVAP (22). This provides a novel signalling response linking environmental perception with organellar dynamics during the developmental cycle of the parasites and provides the earliest yet identified event in the initiation of trypanosome differentiation.

Results

TbPIP39 redistributes during synchronous differentiation

TbPIP39 is expressed in stumpy forms but not slender forms, and is maintained in established procyclic forms in glycosomes (17). To assay the recruitment of TbPIP39 to glycosomes during differentiation we analysed parasites undergoing synchronous development from stumpy to procyclic forms. Specifically, a stumpy enriched (80-90%) population was stimulated to undergo differentiation by exposure to 6mM *cis*-aconitate *in vitro*. Interestingly, the stumpy form location of TbPIP39 was distinct from that of the glycosomal marker protein glycosomal triosephosphate isomerase (gTIM). Rather than being detected in a punctate location throughout the cell typical of glycosomal staining, there was a concentration of staining close to the enlarged flagellar pocket, positioned between the nucleus and kinetoplast of the cell (Figure 1A). In contrast, procyclic forms exhibited the expected distribution of TbPIP39, where co-localisation with both glycosomal aldolase and gTIM was evident. To quantitate this location, slender, stumpy and procyclic form parasites were co-stained for TbPIP39 and gTIM, or for aldolase and gTIM and analysed by confocal microscopy, with co-localisation determined by global Pearson correlation using Volocity software (Figure 1B). This confirmed that aldolase and gTIM showed correlation of >0.8 in each life cycle stage consistent with the ubiquitous expression of these marker glycosomal proteins. In contrast, the correlation of TbPIP39 and gTIM was less than 0.15 in slender forms (where TbPIP39 is not expressed at significant levels), and less than 0.2 in stumpy forms (where TbPIP39 is expressed), whilst in procyclic forms the correlation was over 0.8 This indicated that TbPIP39 may be recruited to glycosomes during the differentiation between bloodstream and procyclic forms.

To analyse the kinetics of recruitment, the distribution of TbPIP39 and gTIM were analysed at time points after exposure of stumpy form parasites to 6mM *cis*-aconitate *in vitro*. Figure 2A, B demonstrates that the periflagellar pocket staining of TbPIP39 was detectable at 0, 20 and 60 minutes following exposure to *cis*-aconitate, but was lost beyond that point. Conversely, a punctate glycosomal signal for TbPIP39 that co-localised with gTIM was detectable by 20 minutes, such that both a glycosomal and periflagellar location was present for TbPIP39 at this early time point. At 60 minutes the periflagellar staining was still detectable on some cells but the glycosomal staining was more emphasised and beyond this timepoint, the staining was mainly glycosomal.

To quantitate the redistribution of the TbPIP39 signal, 250 cells were scored at each time point after exposure to *cis*-aconitate and the parasites assayed for signal either at the periflagellar pocket region alone, at the periflagellar pocket region and glycosomes or in glycosomes alone. Figure 3A demonstrates that there was a transition during differentiation, with a predominantly glycosomal signal evident at 30 minutes and beyond in the differentiation time course. In contrast, parasites maintained *in vitro* at 27 ^{o}C without *cis*-aconitate retained the signal close to the flagellar pocket, although there was also some glycosomal staining evident in some (20-50%) of the cells at 20 minutes and beyond. However, few (5%) cells exhibited only glycosomal staining, unlike when differentiation was stimulated with *cis*-aconitate, where >95% exhibited exclusively glycosomal location at 24h. A global Pearson correlation analysis of parasites undergoing differentiation demonstrated that the colocalization of TbPIP39 and gTIM increased from around 30% at 30 minutes to nearly 80% at 120 minutes, highlighting the rapidity of the redistribution. In contrast, in the absence of *cis*-aconitate, the correlation never exceeded 40% (Figure 3B). The correlation between aldolase and gTIM in the same analysis in contrast was consistently above 80%

demonstrating the stability of the co-localisation between these glycosomal markers through the differentiation time course.

Cytological analysis of the periflagellar staining of TbPIP39 in stumpy and differentiating cells

To examine the unusual periflagellar pocket location of TbPIP39 in stumpy forms more closely, we carried out confocal microscopy to visualise the three-dimensional distribution of TbPIP39 at 30 minutes after exposure to *cis*-aconitate. Figure 3C shows the concentration of the TbPIP39 around the flagellar pocket of the cell. As expected at 30 minutes after exposure to *cis*-aconitate, TbPIP39 was also detected in the glycosomal material anterior of the nucleus. Cells were also examined by deconvolution fluorescence microscopy after labelling for TbPIP39 and the lysosomal marker, p67 (Figure 4A). This again demonstrated the periflagellar pocket location of TbPIP39 but revealed that the signal was not evenly distributed around the flagellar pocket periphery but rather concentrated at discrete foci around the pocket. Furthermore, in cells where the flagellar pocket was collapsed during fixation, the TbPIP39 focused to a tight point supporting the distribution of the signal around, not in the flagellar pocket (Figure 4B). The site of TbPIP39 localisation was also investigated by immunoelectron microscopy (Figure 5A-E). Although signal was not abundant we were able to detect clusters of TbPIP39 labelling within the lumen of membrane bound structures and at vesicle membranes distinct from the flagellar pocket membrane and close to glycosomes in this region of the cell.

Finally, to evaluate whether the periflagellar pocket location of TbPIP39 was an artefact of indirect immunofluorescence we generated cell lines with TbPIP39 fused to mNeon (Figure S1A) and used live cell imaging to detect the fluorescent protein in stumpy

forms restrained in a hydrogel matrix. Figure S1B (movie S1A) revealed that in stumpy forms the fluorescent protein localised at the same periflagellar pocket site as previously visualised by immunofluorescence microscopy, a profile also seen with a YFP-TbPIP39 fusion protein (shown later in Figure 7C). Moreover, the signal redistributed to glycosomes in parasites exposed to *cis*-aconitate for 2 h, and 24 h (movie S1B, movie S1C).

Combined our results demonstrated that TbPIP39 was positioned close to, but not in, the flagellar pocket of the stumpy form parasites and distributed to glycosomes within 1-2h of the initiation of their differentiation to procyclic forms.

Glycosomal dynamics during differentiation upon TbPIP39 depletion

During differentiation between stumpy forms and procyclic forms there is turnover of the glycosomal population presumably contributing to the metabolic adaptation of the parasites as they enter the tsetse fly. To determine whether TbPIP39 recruitment contributed to the control of glycosomal turnover and maturation during differentiation, we analysed the distribution of glycosomal aldolase and the lysosomal marker p67 during differentiation with TbPIP39 either depleted or not by RNAi. Previously, lysosomal and glycosomal staining patterns during differentiation have been subjectively categorised according to the distribution of aldolase and p67 in several cytological subtypes (A-E)(23). To determine if glycosomal/lysosomal dynamics were perturbed by reduced TbPIP39 recruitment during differentiation, pleomorphic *T. brucei* EATRO 1125 AnTat1.1. 90:13 bloodstream form parasites - competent for stumpy formation and inducible RNA interference - were generated able to deplete TbPIP39 under doxycycline regulation. When grown in mice provided either with or without doxycycline in their drinking water, uniform populations of stumpy forms were generated where TbPIP39 mRNA was targeted for RNAi, or not. In mice, the low levels

of TbPIP39 were not significantly further reduced by RNAi and normal differentiation to stumpy forms occurred, as previously seen (18). However, when these stumpy form populations were induced to differentiate to procyclic forms with *cis*-aconitate, the normal increase of TbPIP39 levels was not observed over 24h, supporting RNAi mediated depletion during differentiation (Figure 6A). Over this period, procyclin expression occurred but was less efficient than in uninduced parasites, highlighting delayed or reduced differentiation with a reduction in TbPIP39, as previously reported (18).

To determine the consequences of TbPIP39 RNAi for the glycosomal and lysosomal configurations, cells were assayed during differentiation for the abundance of each glycosomal/lysosomal category (A to E) subjectively defined by (23) (Figure 6B). We observed no clear change in the distribution of the glycosome and lysosomal signal either in the presence or absence of *cis*-aconitate, or when TbPIP39 was depleted or not. The differentiated cells were also allowed to proliferate as procyclic forms for five days after the initiation of differentiation with TbPIP39 RNAi depletion maintained or not with doxycycline. Figure 6C demonstrates that although TbPIP39 remained significantly reduced with RNAi induction in the differentiated procyclic cells, these grew at an equivalent level to cells where TbPIP39 was not depleted.

We conclude that preventing the accumulation of TbPIP39 by RNAi does not significantly alter the changes in the glycosomal dynamics during differentiation from stumpy forms to procyclic forms. Moreover, differentiated procyclic forms do not require abundant TbPIP39 to sustain *in vitro* growth. Instead the dominant function of TbPIP39 under the growth conditions used appears to be restricted to regulating the efficiency of differentiation between bloodstream and procyclic forms.

TbPTP1 and REG9. 1 localise close to TbPIP39 in stumpy forms

TbPIP39 is negatively regulated by the tyrosine phosphatase TbPTP1 that acts as an inhibitor of differentiation in stumpy forms. Previously, TbPTP1 had been difficult to localise using antibody specific for that molecule (16), and so we clarified its localisation with respect to TbPIP39 using an inducible N-terminally Ty1 epitope tagged copy (Figure 7A). Here, TbPTP1 was detected at the discrete periflagellar pocket location, with TbPIP39 co-labelling confirming that the location of the two signalling phosphatases was coincident in stumpy forms (Figure 7B). After 1h exposure to *cis*-aconitate, TbPIP39 relocated to glycosomes as seen earlier, whereas TbPTP1 became more diffuse at the periflagellar pocket site and by 4 h the signal was distributed throughout the cell body in the differentiating cells.

The TbPIP39/TbPTP1 node was also similar to the location of REG9.1, a regulator of stumpy specific transcripts previously observed at the periflagellar pocket region of stumpy forms, in addition to along the flagellum or FAZ (26). Therefore, we colocalised REG9.1 with TbPIP39 using a REG9.1 specific antibody and YFP-tagged TbPIP39 during differentiation and observed redistribution form the periflagellar pocket node to the cytoplasmic distribution previously in stumpy forms within 4 h (Figure 7C). Hence, TbPTP39, TbPTP1 and REG9.1 are all colocalised in stumpy forms at the same cellular site before their redistribution and separation at the onset of differentiation.

The periflagellar location of TbPIP39 and TbPTP1 coassociates with flagellar pocket ER.

The observed location of TbPIP39 in stumpy forms was reminiscent of a specialised region of the ER at the flagellar pocket identified by electron tomography of procyclic form cells (22). This region of the cell is defined by the presence of TbVAP, a flagellum

attachment zone (FAZ) ER membrane contact protein. TbVAP depletion by RNAi in procyclic forms results in loss of the FAZ ER and flagellar pocket ER, but no detectable growth deficit (22). To determine if the TbPIP39 location in stumpy forms associated at the flagellar pocket ER, we colocalised TbPIP39 with TbVAP detected by its incorporation of N terminal mNEON Ty1 epitope tag and expression in pleomorphic cells. Figure 8A demonstrates that the TbPIP39 and TbVAP signals are closely-located in the flagellar pocket region of stumpy forms, but not completely coincident, with TbPIP39 sometimes between two separated TbVAP foci. Matching previous analysis in procyclic form cells (22), TbVAP signal also extended along the flagellum attachment zone with further staining in the cell body.

To explore the association of TbPIP39 and TbVAP at this periflagellar pocket location in more detail, we exploited CRISPR to delete the TbVAP gene in pleomorphic bloodstream form trypanosomes (24). Thus, the Cas9 expressing cell line *T. brucei* EATRO 1125 AnTat90:13 J1339 (25) was transfected with repair templates targeted to the TbVAP gene genomic location, and mutants were isolated (Figure S2A). The resulting cell lines were found to retain a TbVAP gene copy despite their successful insertion of the drug resistance gene (Figure S2B); further attempts to delete the remaining allele were unsuccessful. These TbVAP depleted cells exhibited stumpy formation *in vivo* with similar kinetics as wild type cells (Figure 8B) allowing the location of TbPIP39 and its relocation after the initiation of differentiation to procyclic forms to be assayed.

In TbVAP single KO stumpy forms, TbPIP39 was detected at the periflagellar pocket location, similar to that seen in wild type parasites. Correspondingly, when cells were induced to differentiate to procyclic forms with *cis*-aconitate, TbPIP39 relocated to glycosomes and the cells expressed procyclin, indicating that TbVAP depletion did not alter glycosomal TbPIP39 loading or differentiation (not shown). However, when the TbVAP

304 single KO cells were analysed after 24h in differentiation conditions (*i.e.* with *cis*-aconitate)
305 the parasites appeared enlarged and rounded and were dying, unlike wild type parasites at this
306 time point (Figure 8C) (mean=82% from an analysis of three independent null mutant lines,
307 versus 13% and 14% in the parental and VAP-Ty1 line, respectively, n=250 cells per sample;
308 Figure 8D). Thus, both alleles of TbVAP are necessary for the viability of differentiating
309 cells, but not for the normal relocation of TbPIP39 early in the process.
310
311

Discussion

The differentiation of African trypanosomes between life cycle stages is enacted rapidly upon transition from the blood of mammalian hosts to the midgut of the tsetse fly. We have shown previously that two phosphatases are important in the signalling of the changes from one environment to the next, TbPTP1 and TbPIP39. Of these TbPIP39 is glycosomal in procyclic forms, signalled through its C terminal PTS 1. Here we show that when first made in stumpy forms, TbPIP39 is not glycosomal but rather is localised at a periflagellar pocket region of the parasite where it colocalises with the differentiation inhibitor, TbPTP1. However, upon reception of the differentiation signal TbPIP39 is rapidly (within approximately 20 minutes) relocated into glycosomes, whereas TbPTP1 becomes dispersed to a non-glycosomal, possibly cytosolic site. It is also coincident with the location of a regulator of stumpy form transcripts, REG9.1. Interestingly, this periflagellar pocket site is close to the specialised FAZ endoplasmic reticulum, defined by TbVAP, that may represent a site of glycosomal biogenesis in the differentiating cells. We propose this molecular node comprising TbPIP39, TbPTP1 and REG9.1 generates a 'stumpy regulatory nexus' (STuRN) where the events initiating differentiation between bloodstream and procyclic forms occur.

The biogenesis of peroxisomes and glycosomes can involve new organelles that arise from pre-existing peroxisomal/glycosomal structures or *de novo* synthesis from the endoplasmic reticulum. However, in eukaryotes subject to environmental change, peroxisome composition can be modulated to allow metabolic adaptation, and this can be achieved by *de novo* loading from the ER (27) as well as the growth and division of existing glycosomes. The dynamics of environmental adaptation in procyclic form parasites have been analysed both during differentiation and upon exposure of procyclic forms to low and high glucose concentrations. In differentiation, autophagy is considered important due to the co-

337 association of lysosomes and glycosomes early in the transition between stumpy and
338 procyclic forms (23). The assessment of this is relatively subjective and we observed limited
339 co-association between the lysosomal marker p67 and glycosomal aldolase during
340 synchronous differentiation, at least in the first 2 hours. In contrast, TbPIP39 relocated from
341 the STuRN to glycosomes within 20 minutes, this region being neither the flagellar pocket
342 lumen or the flagellar pocket membrane. Instead the STuRN was adjacent to a specialised
343 region of the endoplasmic reticulum that has been visualised by electron tomography of
344 procyclic forms cells (22) and is also the site of ER concentration in procyclic forms in low
345 glucose. In this region of the cell, ER is associated with both the flagellar pocket and
346 flagellum attachment zone, the region being defined by TbVAP, an orthologue of VAMP
347 associated protein. This molecule is proposed to co-ordinate ER in this region of the cell
348 through linking the specialised four microtubules positioned at the flagellar pocket region of
349 the cytoskeleton to the endoplasmic reticulum or controlling interaction between central ER
350 and the flagellar pocket associated ER. In a previous study, procyclic form viability was not
351 compromised by efficient RNA interference targeting TbVAP suggesting that it is not
352 essential or that significant depletion of its protein levels after RNA interference does not
353 compromise cell viability and replication. By CRISPR/Cas9 mediated gene deletion we also
354 found that bloodstream forms were viable after the deletion of one allele although both alleles
355 could not be deleted. This may reflect that the protein is essential, contrasting with RNAi-
356 depletion experiments, although technical reasons cannot be excluded. Interestingly, however
357 the TbVAP single KO mutants – although able to initiate differentiation between stumpy and
358 procyclic forms - lost cell integrity after 24h, and appeared swollen and balloon like. This
359 suggests that the levels of this molecule are important during differentiation.

360 Our data invoke a model where in stumpy forms TbPIP39 is poised for glycosome
361 recruitment through its recruitment to the STuRN in a pre-glycosomal concentration similar

362 to pre-peroxisomal vesicles (Figure 9). At this site, the presence of TbPTP1 inhibits its
363 activity. With the initiation of differentiation however, TbPTP1 is inactivated and the
364 TbPIP39 protein is activated by phosphorylation through the activity of an -as yet-
365 unidentified kinase and assembled into glycosomes where it can no longer be accessed by
366 TbPTP1. Removing the inhibitor TbPTP1 from its substrate, TbPIP39, renders the
367 differentiation signalling irreversible - a commitment event that has been mapped to
368 approximately 1 hour after exposure to citrate/*cis*-aconitate (18, 28), coincident with the
369 dispersal of TbPIP39 and TbPTP1 in differentiating cells. The glycosomal pool rapidly turns
370 over through autophagy during differentiation, but the loading of new glycosomes generated
371 at the flagellar pocket region allows the remodelling of the glycosomal pool to its procyclic
372 composition. It remains to be established whether TbPIP39 activity is necessary in the mature
373 glycosomes that arise during differentiation or in procyclic forms, since TbPIP39 RNAi did
374 not affect the growth of differentiated cells *in vitro*. It will be interesting to explore the fitness
375 of procyclic forms depleted of TbPIP39 in different culture conditions more closely
376 mimicking conditions in the fly gut, such as when alternative carbon sources are available
377 (29, 30).

378 The synchronous differentiation of trypanosome parasites and their developmental
379 adaptation of glycosomal composition provides a unique capability to explore the dynamics
380 of organellar development in an evolutionary divergent eukaryotic model. This study
381 provides the first temporal and positional tracking of signalling molecules, organellar
382 compartments and contact points at the STuRN, a potential site of glycosomal
383 biogenesis/regeneration as the parasite initiates its metabolic adaptation to a nutritionally
384 distinct environment. Coupled with the high definition understanding of the structural
385 organisation and cytoskeletal interactions in this region of the highly-ordered parasite cell

386 (31-33), trypanosomes provide an invaluable model for the precise regulation and kinetics of
387 inter-organellar exchange in a eukaryotic cell.
388
389
390 **Acknowledgements**
391
392 We thank Professor Paul Michels, University of Edinburgh, for advice and constructive
393 comments on the manuscript. DVS was supported by Erasmus+Mobility grant. DRR was
394 supported by internal grants (CNRS and university of Bordeaux) and support from the ANR,
395 LABEX ParaFrap, ANR-11-LABX-0024 (http://www. labex-parafrap.fr/fr). ME is supported
396 by DFG grants EN305, GRK2157 and SPP1726. Research in KRM's laboratory is funded by
397 a Wellcome Trust Investigator award (103740/Z14/Z) and Royal SocietyWolfson Research
398 Merit award (WM140045).
399 The funders had no role in study design, data collection and interpretation, or the decision to
400 submit the work for publication.

401 **Materials and Methods**

402

403 **Parasites**

404 ***Cell lines and culturing in vitro***

405 Pleomorphic *Trypanosoma brucei* EATRO 1125 AnTat1.1 90:13 (TETR T7POL NEO HYG)
406 (19) and EATRO AnTat 1.1 J1139 (25) parasites were used throughout.
407 Pleomorphic bloodstream and double marker 29-13 procyclic form trypanosomes (34) were
408 cultured *in vitro* in HMI-9 (35) medium at 37^{o}C 5% CO2 or in SDM-79 (36) medium at 27^{o}C
409 respectively.
410 The following selective drugs were used:
411 Hygromycin (2.5 μG/mL), Puromycin (0.5 μG/mL) and Blasticidin (2.5 μG/mL).

412

413 ***In vivo studies***

414 Trypanosome infections were carried out in female healthy outbred MF1 mice at least 10
415 weeks old, immunocompromised with 25mg/ml cyclophosphamide delivered
416 intraperitoneally 24 h prior to trypanosome infection.

417

418 No blinding was performed and the animals were not subject to previous procedures or drug
419 treatment. Animal experiments were carried out according to the United Kingdom Animals
420 (Scientific Procedures) Act under a license (PPL60/4373) issued by the United Kingdom
421 Home Office and approved by the University of Edinburgh local ethics committee. Animals
422 were kept in cages containing 1-5 mice on a 12h daylight cycle and maintained at room
423 temperature.

424

425 *In vivo* growth involved intraperitoneal injection of 10^5 parasites into cyclophosphamide-
426 treated mice and the course of parasitaemia was recorded by performing daily tail-snips to
427 estimate parasite numbers using a 'rapid matching' method involving visual comparisons of
428 live parasites in blood by microscopy with a published standardized chart of parasite numbers
429 per ml (37).
430
431 Ectopically expressed gene expression was induced by inclusion of doxycycline (200 mg/mL
432 in 5% sucrose) in the drinking water, with control mice being provided with 5% sucrose
433 alone. Between 2 and 3 mice were used per group.
434
435 Stumpy-enriched populations were obtained 6–7 d after infection by DEAE cellulose
436 purification (38).
437
438 For the initiation of differentiation conditions were used as described in (17).
439
440 ***Parasite transfection***
441 Parasite transfection was by Amaxa nucleofection according to previous detailed methods for
442 pleomorphic (39) and 29-13 procyclic form parasites (40).
443
444 **Plasmid construction and cell line generation**
445 ***Generating endogenously tagged TbPIP39 pleomorph cell lines***
446 Primers 1.-4. were used to endogenously tag the N-terminus of TbPIP39 using pPOTv4YFP
447 and pPOTv6 mNEONgreen plasmids according to (41).
448
449 ***Generating endogenously tagged TbPTP1 pleomorph cell lines***

The TbPTP1 open reading frame was amplified from *T. brucei* EATRO 1125 AnTat1.1 wild-type genomic DNA by PCR using Primer 5 and Primer 6 (Table S1) with SpeI and Bgl II restriction sites for insertion into the pDex577-Y vector (42) for tetracycline-inducible overexpression with an N-terminal Ty1 epitope tag. The resulting overexpression constructs were linearized with NotI and transfected into *Trypanosoma bucei* EATRO 1125 AnTat1.1 90:13 pleomorphs cells. Several independent cell lines were isolated and their growth analyzed *in vitro* or *in vivo* in the presence or absence of tetracycline, or doxycycline, respectively. Expression was confirmed by Western blotting using an anti-Ty1 antibody.

Generating endogenously tagged and knockout TbVAP pleomorph cell lines

The LeishGEdit program was used (24) to design oligonucleotide primers (Table S1 Primers 7-11) to produce DNA fragments and sgRNAs for the production of Ty1 mNEONGreen tagged VAP and KO VAP cell lines. To create the KO and endogenously tagged pleomorph cell lines EATRO AnTat 1.1 J1139 cells were transfected as described in(25).

Several independent cell lines were isolated and their growth analyzed *in vitro* or *in vivo*. Pleomorph cell lines with the mNEON-Ty1 tagged TbVAP was identified by Western blotting and immunofluorescence using an anti-Ty1 antibody.

Several TbVAP knockout cell line candidates were isolated, and genomic DNA were purified (QIAGene GenomicDNA kit). The genomic DNAs were used in PCR reactions to confirm the presence of the Blastocidine drug resistance cassette (replacing the endogenous TbVAP) (Table S1 primers 7-10) and also the lack of the endogenous TbVAP gene (Table S1 primers 14-15). TbPIP39 RNAi lines were described in (17).

Western blotting, immunofluorescence and confocal, Immuno Electronmicroscopy and live cell microscopy

475

476 Protein expression analyses by Western blotting were carried out according to (17) with
477 antibody concentrations detailed in Table S2.

478

479 Approximately $1x10^9$ EATRO AnTat1.1 90:13 stumpy (around 90-95% cells of the isolated
480 cells were stumpy forms, the rest were intermediates) cells from mice were purified on DE52
481 column in PSG buffer. After purification, cells were resuspended in HMI9 at $4x10^6$/ml and
482 left in a 37°C CO_2 incubator for 60 mins to recover. Then the culture was divided into two
483 aliquots and ~$5x10^8$ stumpy cells treated with *cis*-aconitate (+ CA sample) and $5x10^8$ stumpy
484 cells left untreated (-CA sample). After 60 mins CA induction cells were harvested by
485 centrifugation, washed in 15 ml of vPBS and repelleted, before resuspension in 10 ml vPBS
486 (2.5 $x10^8$ cells/10 ml). Immunofluorescence was carried out according to (20) using the
487 antibody concentrations in Table S2. Phase–contrast and Immunofluorescence microscopy
488 images were captured on a Zeiss axioskop2 (Carl Zeiss microimaging) with a Prior Lumen
489 200 light source using a QImaging Retiga 2000RCCD camera; the objective was a Plan
490 Neofluar ×63 (1.25 NA). Images were captured via QImage (QImaging). Cells were captured
491 for confocal microscopy or processed for immunoelectron or live cell microscopy as
492 described in Text S1.

493

494

References

1. Wu H, Carvalho P, Voeltz GK. 2018. Here, there, and everywhere: The importance of ER membrane contact sites. Science 361.
2. Eden ER, White IJ, Tsapara A, Futter CE. 2010. Membrane contacts between endosomes and ER provide sites for PTP1B-epidermal growth factor receptor interaction. Nat Cell Biol 12:267-72.
3. Allmann S, Bringaud F. 2017. Glycosomes: A comprehensive view of their metabolic roles in T. brucei. Int J Biochem Cell Biol 85:85-90.
4. Bauer S, Morris MT. 2017. Glycosome biogenesis in trypanosomes and the de novo dilemma. PLoS Negl Trop Dis 11:e0005333.
5. Kennedy PG. 2013. Clinical features, diagnosis, and treatment of human African trypanosomiasis (sleeping sickness). Lancet Neurol 12:186-94.
6. Giordani F, Morrison LJ, Rowan TG, HP DEK, Barrett MP. 2016. The animal trypanosomiases and their chemotherapy: a review. Parasitology 143:1862-1889.
7. Bringaud F, Riviere L, Coustou V. 2006. Energy metabolism of trypanosomatids: adaptation to available carbon sources. Mol Biochem Parasitol 149:1-9.
8. Silvester E, McWilliam KR, Matthews KR. 2017. The Cytological Events and Molecular Control of Life Cycle Development of Trypanosoma brucei in the Mammalian Bloodstream. Pathogens 6.
9. Vickerman K. 1965. Polymorphism and mitochondrial activity in sleeping sickness trypanosomes. Nature 208:762-6.
10. Brown RC, Evans DA, Vickerman K. 1973. Changes in oxidative metabolism and ultrastructure accompanying differentiation of the mitochondrion in Trypanosoma brucei. Int J Parasitol 3:691-704.
11. van Grinsven KW, Van Den Abbeele J, Van den Bossche P, van Hellemond JJ, Tielens AG. 2009. Adaptations in the glucose metabolism of procyclic Trypanosoma brucei isolates from tsetse flies and during differentiation of bloodstream forms. Eukaryot Cell 8:1307-11.
12. Dewar CE, MacGregor P, Cooper S, Gould MK, Matthews KR, Savill NJ, Schnaufer A. 2018. Mitochondrial DNA is critical for longevity and metabolism of transmission stage Trypanosoma brucei. PLoS Pathog 14:e1007195.

13. Vassella E, Reuner B, Yutzy B, Boshart M. 1997. Differentiation of African trypanosomes is controlled by a density sensing mechanism which signals cell cycle arrest via the cAMP pathway. J Cell Sci 110 (Pt 21):2661-71.
14. Matthews KR, Gull K. 1994. Evidence for an interplay between cell cycle progression and the initiation of differentiation between life cycle forms of African trypanosomes. J Cell Biol 125:1147-56.
15. Ziegelbauer K, Quinten M, Schwarz H, Pearson TW, Overath P. 1990. Synchronous differentiation of Trypanosoma brucei from bloodstream to procyclic forms in vitro. Eur J Biochem 192:373-8.
16. Szoor B, Wilson J, McElhinney H, Tabernero L, Matthews KR. 2006. Protein tyrosine phosphatase TbPTP1: a molecular switch controlling life cycle differentiation in trypanosomes. J Cell Biol 175:293-303.
17. Szoor B, Ruberto I, Burchmore R, Matthews K. 2010. A novel phosphatase cascade reglates differentiation in trypanosomes via a glycosomal signaling pathway. Genes and Development 24:1306-1316.
18. Szoor B, Dyer N, Ruberto I, Acosta Serrano A, K. M. 2013. Independent pathways can transduce the life-cycle differentiation signal in Trypanosoma brucei. PLOS Pathogens 10.1371/journal.ppat.1003689.
19. Engstler M, Boshart M. 2004. Cold shock and regulation of surface protein trafficking convey sensitization to inducers of stage differentiation in Trypanosoma brucei. Genes Dev 18:2798-811.
20. Dean S, Marchetti R, Kirk K, Matthews KR. 2009. A surface transporter family conveys the trypanosome differentiation signal. Nature 459:213-7.
21. Colasante C, Ellis M, Ruppert T, Voncken F. 2006. Comparative proteomics of glycosomes from bloodstream form and procyclic culture form Trypanosoma brucei brucei. Proteomics 6:3275-93.
22. Lacomble S, Vaughan S, Deghelt M, Moreira-Leite FF, Gull K. 2012. A Trypanosoma brucei protein required for maintenance of the flagellum attachment zone and flagellar pocket ER domains. Protist 163:602-15.
23. Herman M, Perez-Morga D, Schtickzelle N, Michels PA. 2008. Turnover of glycosomes during life-cycle differentiation of Trypanosoma brucei. Autophagy 4:294-308.

24. Beneke T, Madden R, Makin L, Valli J, Sunter J, Gluenz E. 2017. A CRISPR Cas9 high-throughput genome editing toolkit for kinetoplastids. R Soc Open Sci 4:170095.
25. Rojas F, Silvester E, Young J, Milne R, Tettey M, Houston DR, Walkinshaw M, Pérez-Pi I, Auer M, Denton H, Smith TK, Thompson J, Matthews KR. 2018. Oligopeptide signaling through TbGPR89 drives trypanosome quorum sensing. Cell, in press.
26. Rico E, Ivens A, Glover L, Horn D, Matthews KR. 2017. Genome-wide RNAi selection identifies a regulator of transmission stage-enriched gene families and cell-type differentiation in Trypanosoma brucei. PLoS Pathog 13:e1006279.
27. Kalel VC, Schliebs W, Erdmann R. 2015. Identification and functional characterization of Trypanosoma brucei peroxin 16. Biochim Biophys Acta 1853:2326-37.
28. Domingo-Sananes MR, Szoor B, Ferguson MA, Urbaniak MD, Matthews KR. 2015. Molecular control of irreversible bistability during trypanosome developmental commitment. J Cell Biol 211:455-68.
29. Wargnies M, Bertiaux E, Cahoreau E, Ziebart N, Crouzols A, Morand P, Biran M, Allmann S, Hubert J, Villafraz O, Millerioux Y, Plazolles N, Asencio C, Riviere L, Rotureau B, Boshart M, Portais JC, Bringaud F. 2018. Gluconeogenesis is essential for trypanosome development in the tsetse fly vector. PLoS Pathog 14:e1007502.
30. Mantilla BS, Marchese L, Casas-Sanchez A, Dyer NA, Ejeh N, Biran M, Bringaud F, Lehane MJ, Acosta-Serrano A, Silber AM. 2017. Proline Metabolism is Essential for Trypanosoma brucei brucei Survival in the Tsetse Vector. PLoS Pathog 13:e1006158.
31. Vaughan S. 2010. Assembly of the flagellum and its role in cell morphogenesis in Trypanosoma brucei. Curr Opin Microbiol 13:453-8.
32. Sun SY, Kaelber JT, Chen M, Dong X, Nematbakhsh Y, Shi J, Dougherty M, Lim CT, Schmid MF, Chiu W, He CY. 2018. Flagellum couples cell shape to motility in Trypanosoma brucei. Proc Natl Acad Sci U S A 115:E5916-E5925.
33. Hoog JL, Bouchet-Marquis C, McIntosh JR, Hoenger A, Gull K. 2012. Cryo-electron tomography and 3-D analysis of the intact flagellum in Trypanosoma brucei. J Struct Biol 178:189-98.
34. Wirtz E, Leal S, Ochatt C, Cross GA. 1999. A tightly regulated inducible expression system for conditional gene knock-outs and dominant-negative genetics in Trypanosoma brucei. Mol Biochem Parasitol 99:89-101.

35. Hirumi H, Hirumi K. 1989. Continuous cultivation of Trypanosoma brucei blood stream forms in a medium containing a low concentration of serum protein without feeder cell layers. J Parasitol 75:985-9.

36. Brun R, Schonenberger. 1979. Cultivation and in vitro cloning or procyclic culture forms of Trypanosoma brucei in a semi-defined medium. Short communication. Acta Trop 36:289-92.

37. Herbert WJ, Lumsden WH. 1976. Trypanosoma brucei: a rapid "matching" method for estimating the host's parasitemia. Exp Parasitol 40:427-31.

38. Lanham SM. 1968. Separation of trypanosomes from the blood of infected rats and mice by anion-exchangers. Nature 218:1273-4.

39. MacGregor P, Rojas F, Dean S, Matthews KR. 2013. Stable transformation of pleomorphic bloodstream form Trypanosoma brucei. Mol Biochem Parasitol doi:S0166-6851(13)00092-3 [pii]
10.1016/j.molbiopara.2013.06.007.

40. Burkard G, Fragoso CM, Roditi I. 2007. Highly efficient stable transformation of bloodstream forms of Trypanosoma brucei. Mol Biochem Parasitol 153:220-3.

41. Dean S, Sunter J, Wheeler RJ, Hodkinson I, Gluenz E, Gull K. 2015. A toolkit enabling efficient, scalable and reproducible gene tagging in trypanosomatids. Open Biol 5:140197.

42. Kelly S, Reed J, Kramer S, Ellis L, Webb H, Sunter J, Salje J, Marinsek N, Gull K, Wickstead B, Carrington M. 2007. Functional genomics in Trypanosoma brucei: a collection of vectors for the expression of tagged proteins from endogenous and ectopic gene loci. Mol Biochem Parasitol 154:103-9.

43. Schindelin J, Arganda-Carreras I, Frise E, Kaynig V, Longair M, Pietzsch T, Preibisch S, Rueden C, Saalfeld S, Schmid B, Tinevez JY, White DJ, Hartenstein V, Eliceiri K, Tomancak P, Cardona A. 2012. Fiji: an open-source platform for biological-image analysis. Nat Methods 9:676-82.

44. Glogger M, Subota I, Pezzarossa A, Denecke AL, Carrington M, Fenz SF, Engstler M. 2017. Facilitating trypanosome imaging. Exp Parasitol 180:13-18.

623 **Figure Legends**

624

625

626 **Figure 1**

627 A. Serial Z stack slices through a stumpy form trypanosome cell stained to localise the
628 differentiation regulator TbPIP39 (green) or glycosomal TIM (red). The cell nucleus
629 and kinetoplast are shown in blue. The TbPIP39 is located close to, but slightly
630 anterior of, the kinetoplast and is not collocated with the glycosomal marker.
631 Bar=5µm.

632 B. Pearson coefficient of colocalisation between TbPIP39 and glycosomal TIM or
633 between aldolase and glycosomal TIM in bloodstream slender and stumpy forms, or
634 in procyclic forms. Colocalisation values were calculated using Volocity software
635 based on captured confocal images. Threshold was set according to background of
636 images.

637

638 **Figure 2**

639

640 A. Representative images of trypanosomes undergoing differentiation from stumpy
641 forms to procyclic forms. Samples were taken at the time points indicated after the
642 initiation of differentiation by *cis*-aconitate. Cells were labelled for the location of
643 TbPIP39 (green) or the glycosomal marker gTIM (red), with the nucleus and
644 kinetoplast being labelled with DAPI (blue). Phase contrast images are shown on the
645 left-hand side and merged images shown on the right. Bar= 10µm.

B. Selected fields of cells stained for TbPIP39, gTIM or DAPI at time points after the initiation of differentiation. The location of TbPIP39 proximally to the flagellar pocket region of the cell is highlighted with arrowheads. Bar=12µm.

Figure 3

A. Quantitation of the distribution of TbPIP39 between the periflagellar pocket location only (green), at the periflagellar pocket and in glycosomes (yellow) or exclusively in glycosomes (red). At each time point and in each condition (with or without *cis*-aconitate, to initiate differentiation), 250 cells were scored.

B. Pearson coefficient of colocalisation between TbPIP39 and glycosomal TIM or between aldolase and glycosomal TIM at time points after the exposure of stumpy forms to *cis*-aconitate. Colocalisation values were calculated using Volocity software based on captured confocal images. The threshold was set according to background of images.

C. 3-D reconstruction of a cell 30 minutes after exposure to *cis*-aconitate and stained for TbPIP39 (green) and glycosomal gTIM (red). The cell nucleus (N) and kinetoplast (K) are labelled blue. TbPIP39 is concentrated around the flagellar pocket of the cell but also shows labelling at a dispersed glycosomal location more anterior in the cell, coincident with the distribution of glycosomal gTIM. Bar=5µm.

Figure 4

A. Co-labelling of stumpy form cells (without exposure to *cis*-aconitate) stained for TbPIP39 (green) and the lysosomal marker p67 (red). The nucleus and kinetoplast are stained in blue. The TbPIP39 labelling is distinct from the lysosome, being positioned

unevenly around the flagellar pocket (cell i) or at a tight focus in cells where the flagellar pocket is collapsed (Cell iii, iv). Cell ii has no staining detected at the flagellar pocket region. Bar=5µm.

B. Co-labelling of stumpy form cells (without exposure to *cis*-aconitate) stained for TbPIP39 (green) and the glycosomal gTIM (red). The flagellar pocket and cell surface membrane are labelled blue with AMCA. Arrows indicate the distribution of the TbPIP39 signal unevenly around the flagellar pocket (Cell *a* image i, ii; Cell *b*, image iii, iv), or at a tight focus associated with a collapsed flagellar pocket (Cell *c*, image iii, iv). Bar=5µm

Figure 5

A-D Immunoelectron micrographs taken of thin sections of the flagellar pocket region of stumpy cells immunogold-labelled for TbPIP39. Arrows indicate the boundary of membrane bound vesicles containing TbPIP39 signal; glycosomes are labelled 'Gl'.

E Immunoelectron micrographs of the flagellar pocket region of stumpy cells in the absence of primary antibody.

Figure 6

A. RNAi depletion of TbPIP39. *T. brucei* EATRO 1125 AnTat1.1 TbPIP39 RNAi cells or *T. brucei* EATRO 1125 AnTat1.1 cells were grown in mice, with or without doxycycline induction. The generated stumpy cells were then exposed, or not, to *cis*-aconitate to initiate differentiation (with doxycyline remaining in the RNAi-induced samples) and TbPIP39 protein detected at 24h. TbPIP39 levels increase during differentiation (ms1, ms2) but this is greatly reduced in induced RNAi samples

(ms3). EF1 alpha provides a loading control, this being a little higher in cells exposed to *cis*-aconitate due to their replication as differentiated procyclic forms. EP procyclin staining shows relative differentiation in the presence or absence of *cis*-aconitate.

B. Distribution of the glycosomal marker aldolase and the lysosomal marker p67 during differentiation between stumpy and procyclic forms. The panel shows the prevalence of different categories of lysosomal/glycosomal staining (as defined by Herman et al., 2008 (Reference [23]), and shown at the left-hand side) at time through differentiation when TbPIP39 was depleted by RNAi or not.

C. Western blot of TbPIP39 in cells differentiated to proliferative procyclic forms with TbPIP39 RNAi induced or not. EF1alpha shows the loading control. The lower panel shows that by day 4 and 5 the cells remain proliferative (the cells were passaged at day 2) despite expressing significantly less TbPIP39.

Figure 7

A. Schematic representation of the construct used to N-terminally tag TbPTP1 with the Ty1 epitope tag.

B. Co-localisation of TbPTP1-ty (green), and TbPIP39 (red) in stumpy forms (0h) and after 1h and 4h exposure to *cis*-aconitate. The TbPTP1 signal is detected as an ectopically expressed copy incorporating an N terminal Ty1 epitope tag to allow its detection. The TbPIP39 signal is detected using an antibody recognising that protein. The cell nucleus and kinetoplast are labelled with DAPI (blue). TbPTP1 colocalised with TbPIP39 in stumpy forms (arrowheads) but after 1h, TbPIP39 has relocated to glycosomes, while TbPTP1 has become more diffuse, albeit some remaining concentrated in the periflagellar pocket region (arrowheads). At 4h, TbPIP39 is glycosomal while TbPTP1 is diffuse throughout the cell body. Bar=10μm.

C. Detection of YFP tagged TbPIP39 (green) in stumpy form cells and its location with respect to REG9.1 (red). DAPI (blue) denotes the position of the cell nucleus and kinetoplast. Bar=15µm.

Figure 8

A. Detection of Ty1 epitope tagged TbVAP in stumpy form cells and its location with respect to TbPIP39. The Ty1 tagged TbVAP (green) is detected at the flagellar pocket region, along the flagellum attachment zone and in the cell body. TbPIP39 (red) is closely proximal at the flagellar pocket region but not precisely coincident. DAPI (blue) denotes the position of the cell nucleus and kinetoplast. Arrowheads indicate the region of TbPIP39. Bar=15µm.

B. Proportion of slender, intermediate and stumpy forms in TbVAP single knock out cells versus parental cells, or epitope tagged TbVAP cells.

C. TbVAP single allele replacement mutants 24h after the initiation of differentiation to procyclic forms. The differentiating cells (indicated by their expression of EP procyclin, green) are swollen and lose integrity. TbPIP39 is punctate throughout the cell, indicating a glycosomal rather than periflagellar pocket distribution. The merged panel shows TbPIP39 (red), EP procyclin (green) and DAPI (blue) revealing the nucleus and kinetoplast. Bar=25µm.

D. Quantitation of cells which exhibit a rounded morphology. Parental *T. brucei* AnTat1.1 J1339 cells, TbVAP1-mNeon-Ty1 expressing cells or three TbVAP single allele deletion mutants are shown. In each case the percentage of rounded cells is

745 shown after 24h either in the absence or presence of *cis*-aconitate as a differentiation
746 stimulus. At least 250 cells were scored for each cell line and each condition.
747
748
749 **Figure 9**
750 Schematic representation of the distribution of gTIM (representing glycosomes)
751 TbPIP39, TbPTP1, TbVAP and REG9.1 in stumpy forms and at 30 minutes and 60
752 minutes after exposure to *cis*-aconitate and in procyclic forms.
753
754

Text S1

Supplementary material and methods

Confocal imaging

Confocal imaging used a Leica SP5 confocal laser scanning microscope, using 63x oil immersion objective (NA = 1.4) and 4.2x digital zoom. The green channel was imaged using a 488-nm argon laser, and the red channel was imaged using a 543-nm helium/neon laser. The final image was acquired using Volocity Software (www.perkinelmer.co.uk) version 4.4. 3D fluorescence microscopy was performed using a fully automated Leica DMI6000B inverse microscope equipped with a 100x (NA 1.4) oil immersion objective and a Leica DFC365 FX CCD camera. Fluorescent and differential interference contrast (DIC) image stacks were acquired by recording stacks of 50 images with a step size of 137 nm. Fluorescent image stacks were deconvolved using Huygens Essential (SVI, Hilversum, Netherlands). Images were visualised as z-stack projections using Fiji(43), or as volumetric representations using Amira (Thermo Fisher Scientific).

Electron microscopy

After incubation of cells in an equal volume of vPBS and 8% paraformaldehyde, cells were pelleted at 1,000x g for 15 min at 4°C. The supernatant was removed and the pellet dehydrated with 30% ethanol at 4°C for 30min. The pellet was then taken through the

779 following series of methanol dehydrations, 60%, 90%, 3 x absolute (30 min each) at -20°C.
780 After dehydration, the pellet was incubated in 2mL of 30% HM20 Lowicryl monostep EM
781 resin (EMS - 14345) in methanol at -20°C, 30min, then taken through increasing
782 concentrations of HM20 (60 min each) then 3 x 100% absolute HM20 at -20°C. The pellet
783 was polymerised at -20°C for 24hr using UV light at 360nm, then left at -20 °C for 24h. The
784 block was cut using a diamond knife and 100nm thin sections were incubated on 100µL
785 droplets of 100mM glycine in PBS 2 x 10 min. Sections were then probed with primary
786 antibody 25µL droplets of rabbit anti-PIP39 diluted 1:100 in incubation buffer (PBS,
787 containing 0.1% Tween 20, 0.1% BSA, pH 7.3), for 2h at room temp. After washing, 4 x 10
788 min in incubation buffer, grids were incubated in a 1:1 mix of protein A (EMS - 25285), plus
789 protein G (EMS - 25315) 10 nm gold, diluted 1:25 in incubation buffer for 2h at room temp.
790 Grids were washed 2 x 10 min in PBS, containing 0.1% Tween 20, 0.1% BSA, pH 7.3, then 2
791 x 10 min in PBS, pH 7.3, then 2 x 10 min in Milli-Q water. Grids were stained in 2% uranyl
792 acetate for 1min at room temp then washed 4 x 10 min in Milli-Q water and visualised on a
793 Technai 12 at 120Kv.

794 **Live cell microscopy**

795

796 ***Sample preparation for live cell microscopy***

797 For studying stumpy to procyclic form differentiation by live cell microscopy 25 µL of
798 pH7.6, 0.6 M, filtered *cis*-aconitate was added to 2.5 ml of stumpy culture ($4x10^6$/ml) to
799 induce differentiation.

800

After 10 mins 1mL sample of the induced culture was taken to concentrate for the hydrogel fixation. Samples were spun for 10 min at 1400 rpm at 37^{o}C and 980 µL supernatants were removed after the spin cells were carefully resuspended in 20 µL culture media.

Immobilisation of living cells was performed with a two component hydrogel, consisting of 8-arm poly ethylene glycol (PEG) norborene and linear PEG-dithiol, essentially as described in (44). 4µl of hydrogel produced with TDB was mixed with a 2 µL solution containing $4x10^5$ differentiating stumpy cells and incubated 1 minute on ice. The mixture was transferred to a glass bottom cell culture dish (FluoroDish, FD35, World Precision Instruments) and allowed to polymerise at room temperature. Cells were viable in the hydrogel for at least 60 minutes (Glogger et al., 2017). In the experiments for this work, the hydrogel concentration was chosen so as to prevent translocation of cells, but still allow flagellar movement. As a control, 100 µL of the induced culture was taken and spun at the same speed and time as the immobilised sample. The cell pellet was carefully resuspended in 1.9 ml of warm TDB ($2x10^5$/ml) and was used to overlay the hydrogel droplet containing *cis*-aconitate induced stumpy cells.

Live imaging was performed with a Leica DMI6000B fully automated inverse microscope equipped with a 100x (NA1.4) oil immersion objective and a pco.edge SCMOS camera (PCO, Kelheim, Germany). Time series were recorded with 100 fps (100 ms resolution), which allowed the accurate detection of dynamic fluorescent signals in the cytoplasm of the living cells. Continuous videos were recorded switching between the fluorescence excitation and DIC settings. Due to the repetitive, periodic beating of the flagellum and cell movement of the immobilised trypanosome, the fluorescent and DIC images of corresponding phase shifted time series could be overlaid using Fiji (Fig. S1B, 0h).

825

826

827

828

829

830 **Table S1. Oligonucleotides used in the study**

831

832

Number	Target gene	Primer name	Primer sequence
1.	PIP39	coding seq amplification Fwd	5’ ggatcaggatcgggtagtatggtgaggacgacacgcttttc 3’
2.	PIP39	coding seq amplification Rev	5’ gagattccaccacgtgcctc 3’
3.	PIP39	5'UTR seq amplification Fwd	5’ atgcgactcttggtctcacc 3’
4.	PIP39	5'UTR seq amplification Rev	5’ gcagcaggtctgcattatacatttcaatgagttccagttggg 3’
5.	PTP1	pDEX577SpeIFwd	5’ ccactagtatgtccacagcgaagagttttccgatggctcaa 3’
6.	PTP1	pDEX577BglIIRev	5’ gggagatctcgcttttaagttaagtgtcgacaccagtcc 3’
7.	VAP	Upstream Fwd	5’ acctgcacaaatatactctgaaagcaaccagtataatgcagacctgctgc 3’
8.	VAP	Upstream Rev	5’ aacagacggtgccgccgttttacttctcatactacccgatcctgatccag 3’
9.	VAP	Downstream Fwd	5’ acgttgttttgctggtggtggtttgcctacggttctggtagtggttccgg 3’
10.	VAP	Downstream Rev Tag	5’ ttctgttctttttttcccccccctctttcctccaatttgagagacctgtgc 3’
11.	VAP	Downstream Rev KO	5’ ttctgttctttttttcccccccctctttcctccggaaccactaccagaacc 3’
12.	VAP	Synthetic single guide RNA 5’	5’ gaaattaatacgactcactataggtatcttacaattttctgcgtgttttagagctagaaatagc 3’
13.	VAP	Synthetic single guide RNA 3’	5’ gaaattaatacgactcactataggagtgagtgtgctttcagaaagttttagagctagaaatagc 3’
14.	VAP	VAP Fwd	5’ actctgaaagcaaccaacgc 3’
15.	VAP	VAP Rev	5’ ccaccaccagcaaaacaacg 3’

833

834 **Table S2: Antibodies used in the study**

Antibody name	Animal raised in	Dilution used on Western Blot (W) or in immuno fluorescence assays (IF)
PIP39	Rb	1:750 W, 1:300 IF
BB2	Ms	1:5 W, 1:4 IF
EF1	Ms	1:7000 W
EP procyclin	Ms	1:3000 W, 1:250 IF
gTIM	Ms	1:500 IF
Aldolase	Ms	1:250 IF
p67	Ms	1:1000 IF
REG 9.1	Rb	1:1000 IF
Alexa568 Red	Ms/Rb	1:500 IF
Alexa488 Green	Ms/Rb	1:500 IF
Licor Red Rb	Ms/Rb	1:7500 W
Licor Green Ms	Ms/Rb	1:7500 W

835

836

Figure S1.

A. Schematic representation of the construct used to N-terminally tag TbPIP39 with mNeon.

B. Video images of TbPIP39 mNeon signal in stumpy forms (0h), or 2h or 24h after exposure to *cis*-aconitate to initiate differentiation. At 0h the signal is predominantly periflagellar pocket, though with some dispersed glycosomal signal. At 2h there is still some periflagellar pocket signal but stronger glycosomal signal. At 24h the signal is exclusively glycosomal. Bar=20µm.

Figure S2

A. Schematic representation of the deletion of TbVAP alleles by CRISPR. The allele was deleted through integration of a blasticidin resistance cassette.

B. PCR analysis of the insertion of a TbVAP replacement construct using CRISPR. All cell lines derived have successfully incorporated the VAP replacement cassette but also retain an intact copy of the TbVAP gene.

A

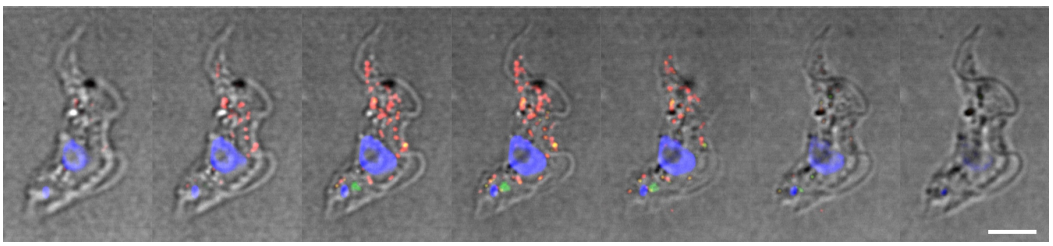

DAPI-TbPIP39-gTIM

B

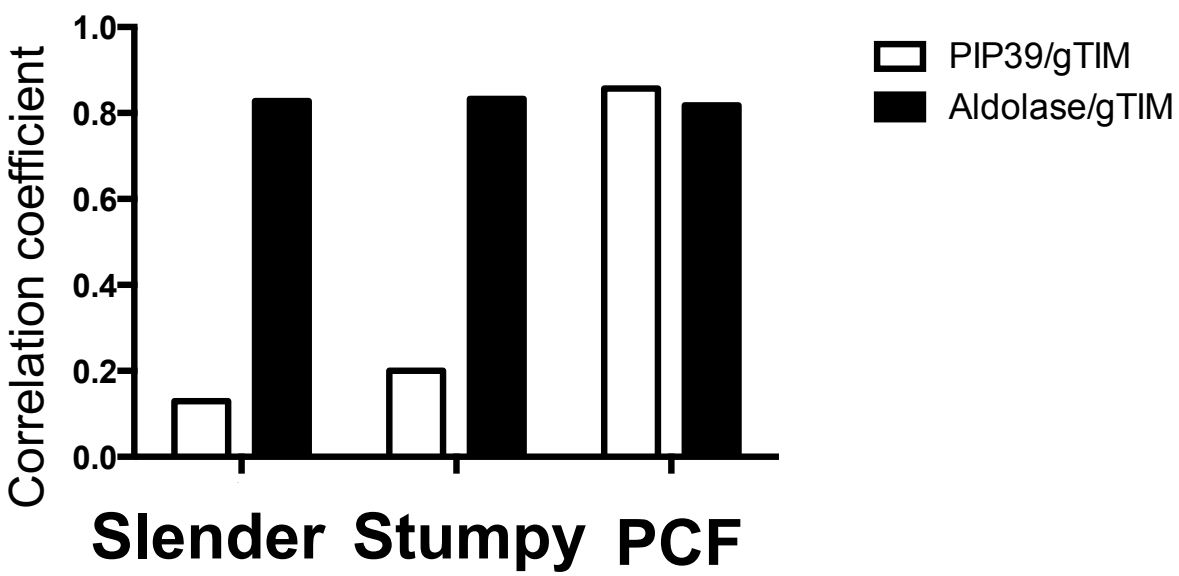

Figure 1

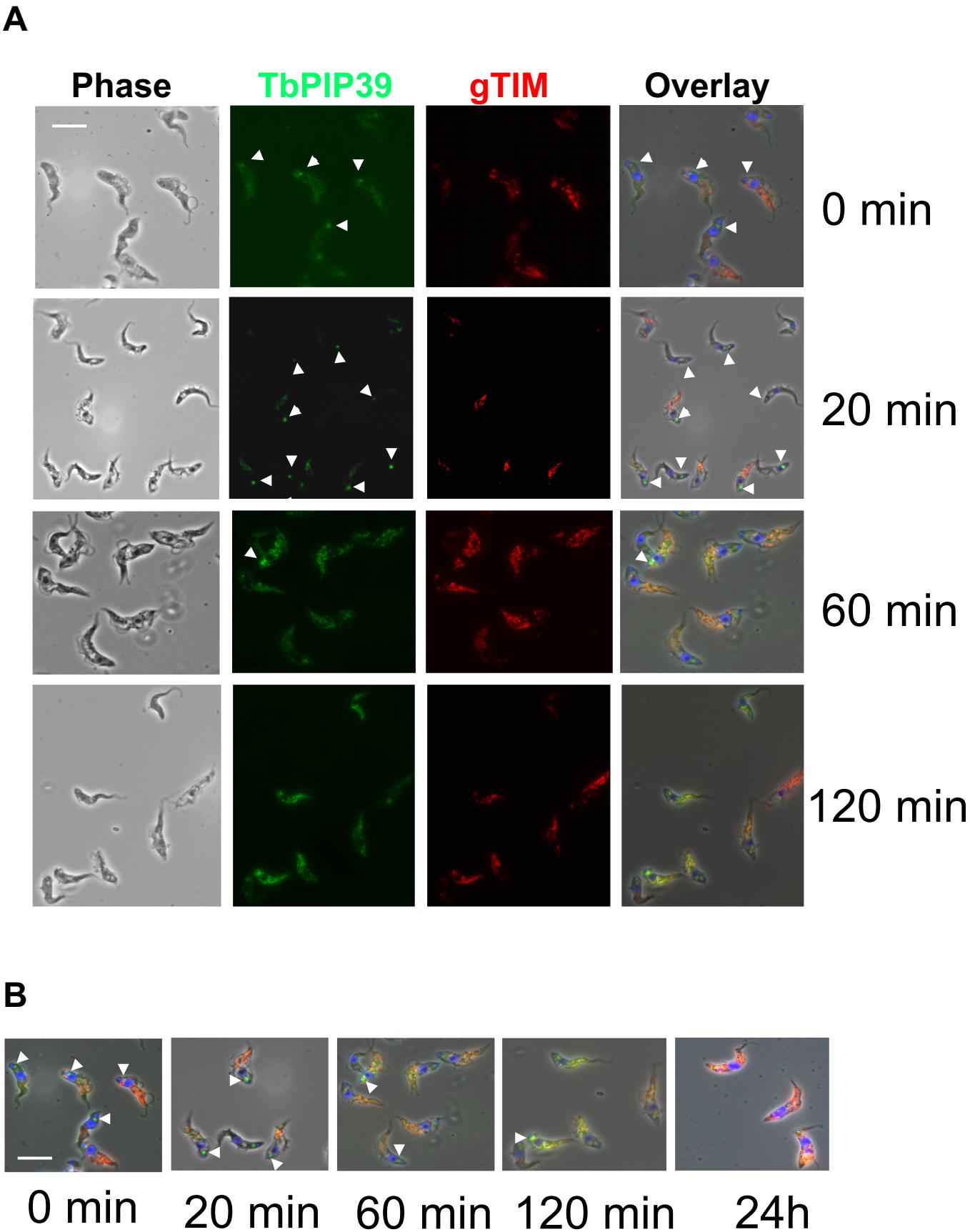
A
Phase
TbPIP39
gTIM
Overlay
0 min
20 min
60 min
120 min
B
0 min
20 min
60 min
120 min
24h

Figure 2

A

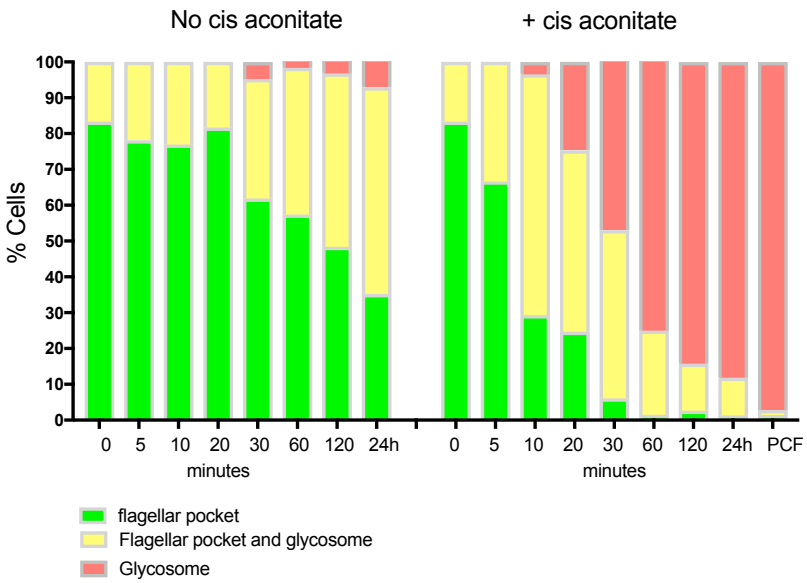
No cis aconitate
+ cis aconitate
% Cells
100
90
80
70
60
50
40
30
20
10
0
0 5 10 20 30 60 120 24h
minutes
0 5 10 20 30 60 120 24h PCF
minutes
flagellar pocket
Flagellar pocket and glycosome
Glycosome

B

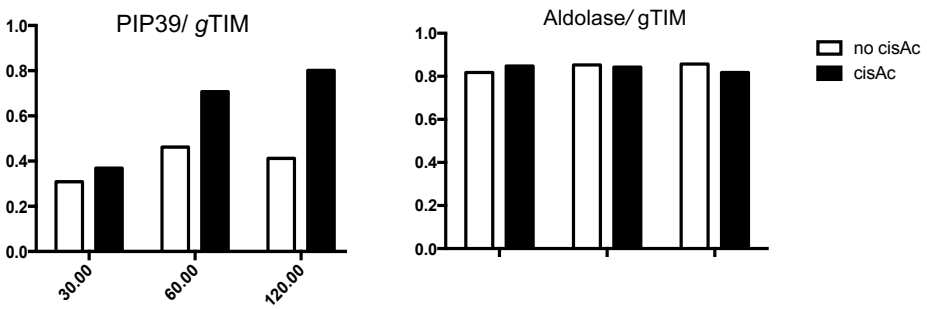
PIP39/ gTIM
Aldolase/ gTIM
1.0
0.8
0.6
0.4
0.2
0.0
30.00
60.00
120.00
no cisAc
cisAc

C

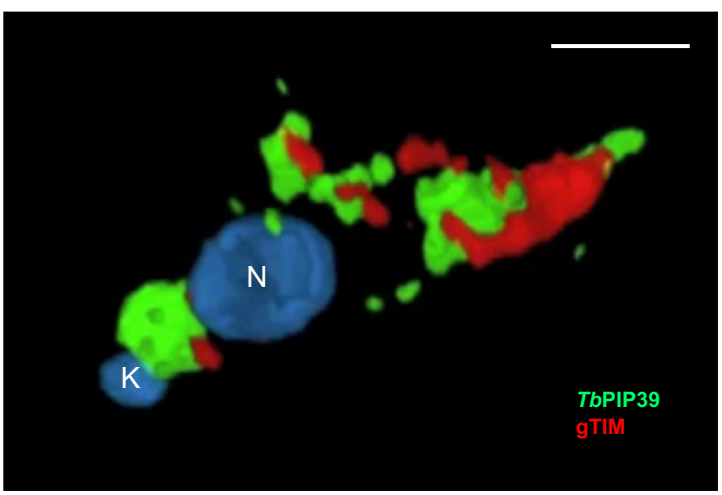
N
K
TbPIP39
gTIM

Figure 3

A

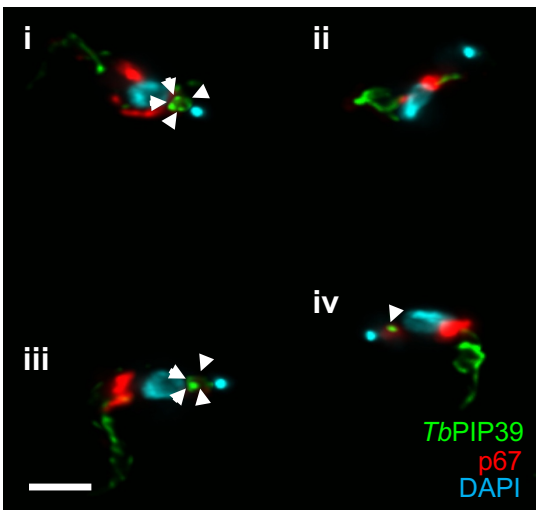

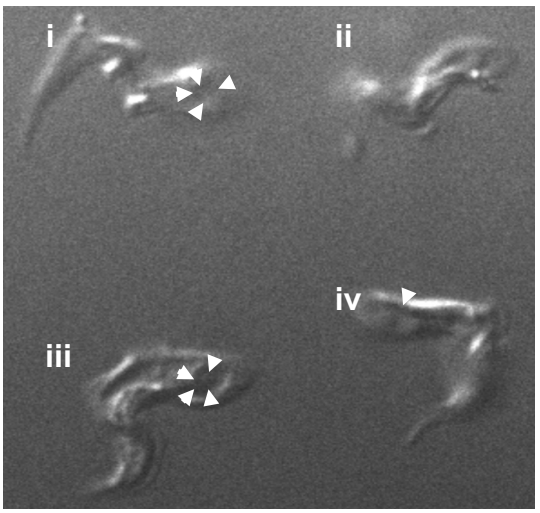

i- Large FP
ii- No Stain around FP
iii- Large FP
iv- collapsed FP

TbPIP39
p67
DAPI

B

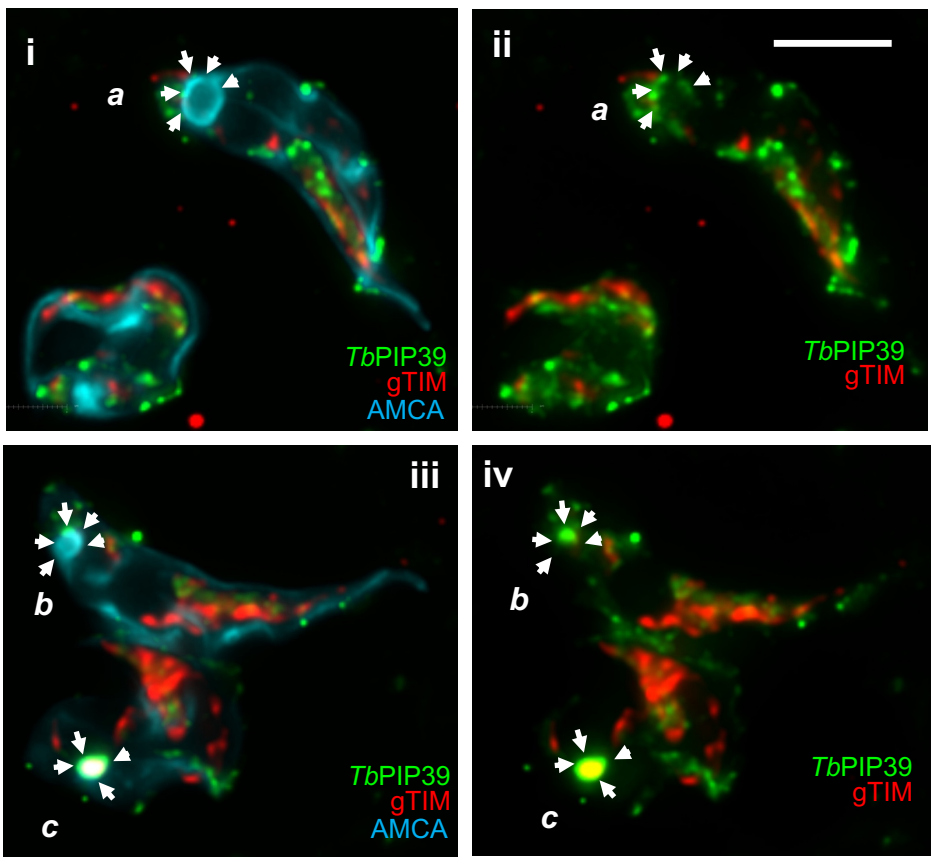

a- Large pocket
b- Medium pocket
c- Collapsed pocket

Figure 4

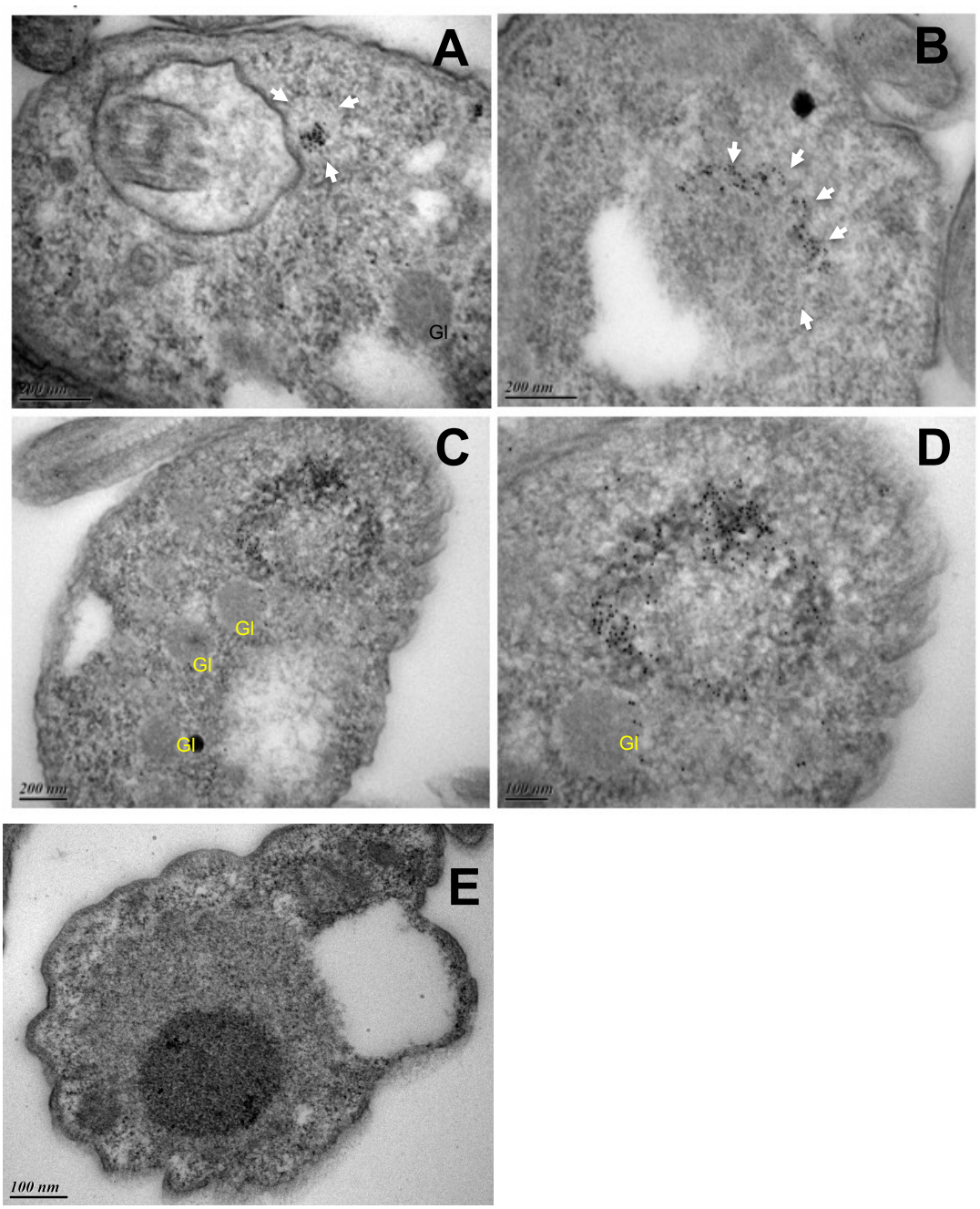

Figure 5

A

PIP39 RNAi induction ablates PIP39

	0 h			24 h					
	Ms1 AnTaT	**Ms2** PIP39 RNAi -	**Ms3** PIP39 RNAi+	**Ms1** AnTaT		**Ms2** PIP39 RNAi -		**Ms3** PIP39 RNAi +	
Dox	+	-	+	+	+	-	-	+	+
CisAc	-	-	-	-	+	-	+	-	+

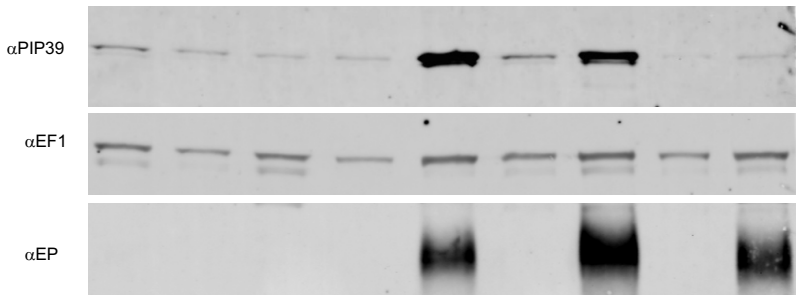

B

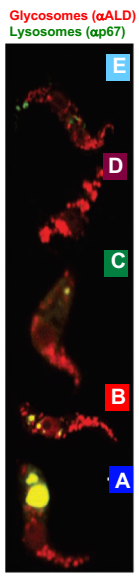

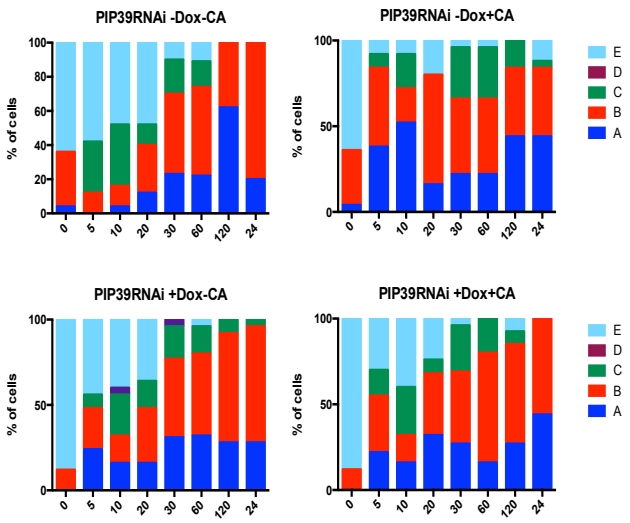

C

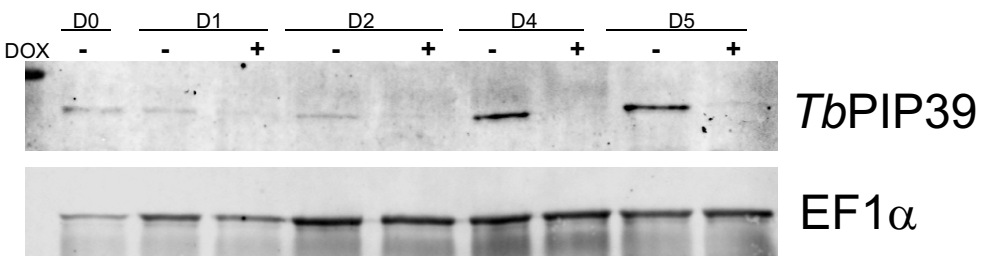

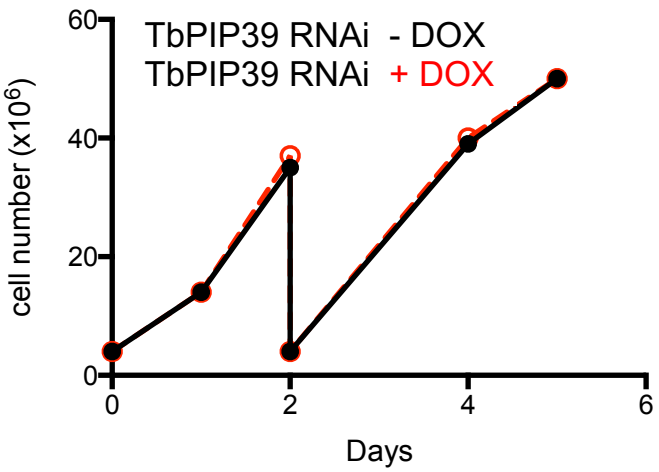

Figure 6

A

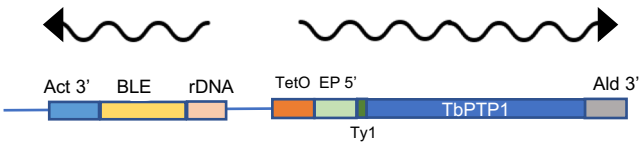
Act 3'
BLE
rDNA
TetO
EP 5'
Ald 3'
TbPTP1
Ty1

B

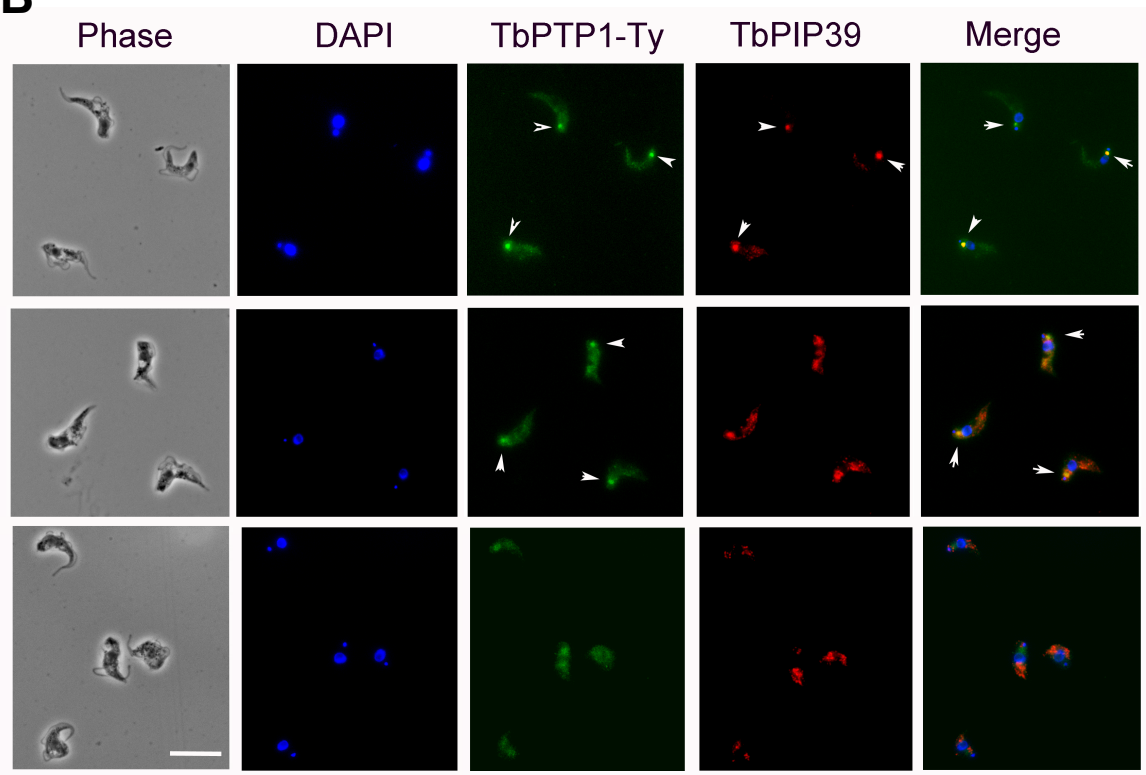
Phase
DAPI
TbPTP1-Ty
TbPIP39
Merge
0h
1h
4h

C

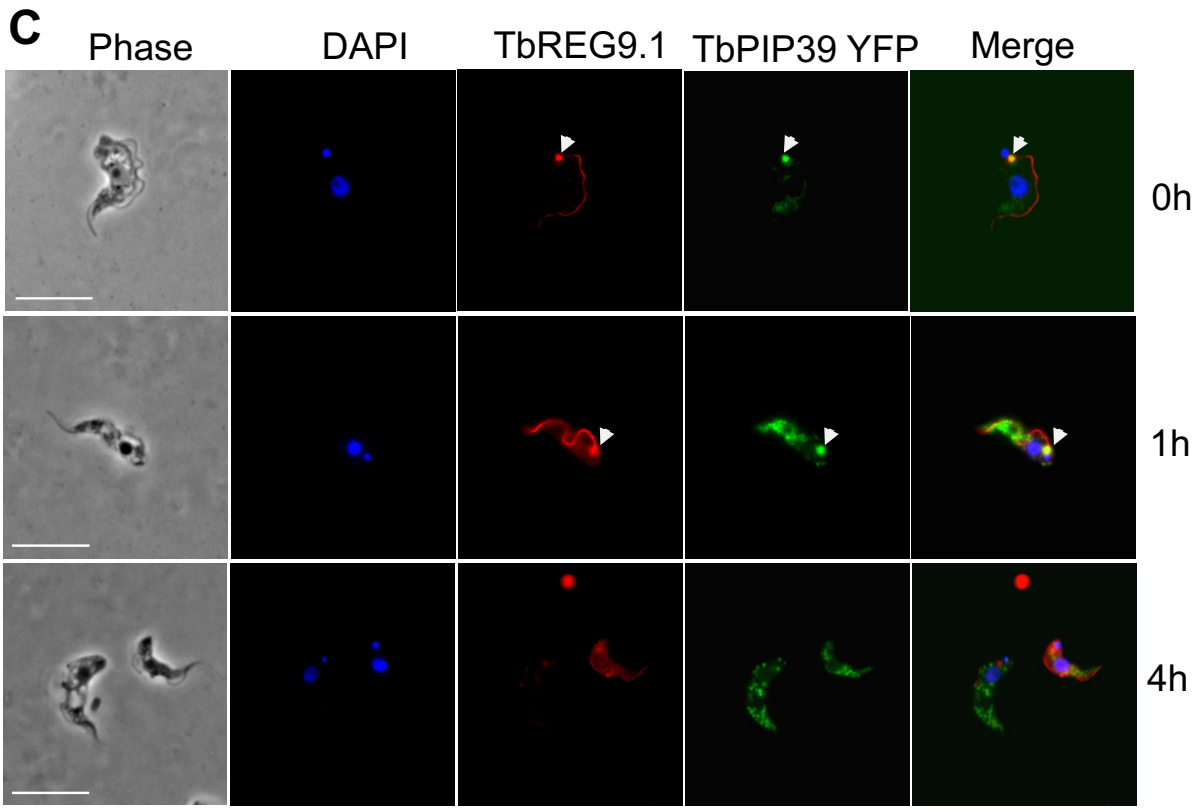
Phase
DAPI
TbREG9.1
TbPIP39 YFP
Merge
0h
1h
4h

Figure 7

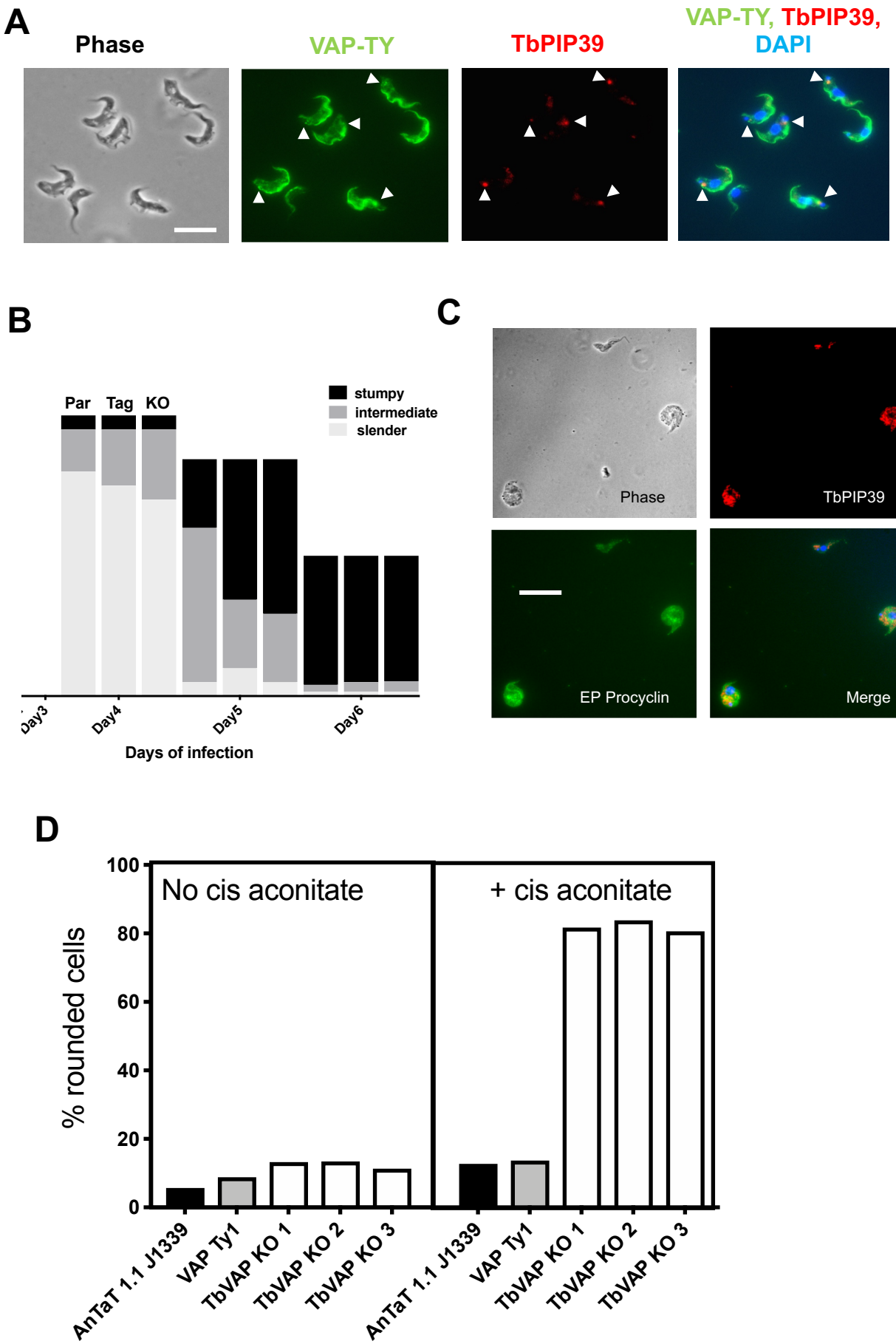
A
Phase
VAP-TY
TbPIP39
VAP-TY, TbPIP39, DAPI
B
Par
Tag
KO
stumpy
intermediate
slender
Day3
Day4
Day5
Day6
Days of infection
C
Phase
TbPIP39
EP Procyclin
Merge
D
% rounded cells
100
80
60
40
20
0
No cis aconitate
+ cis aconitate
AnTaT 1.1 J1339
VAP Ty1
TbVAP KO 1
TbVAP KO 2
TbVAP KO 3
AnTaT 1.1 J1339
VAP Ty1
TbVAP KO 1
TbVAP KO 2
TbVAP KO 3

Figure 8

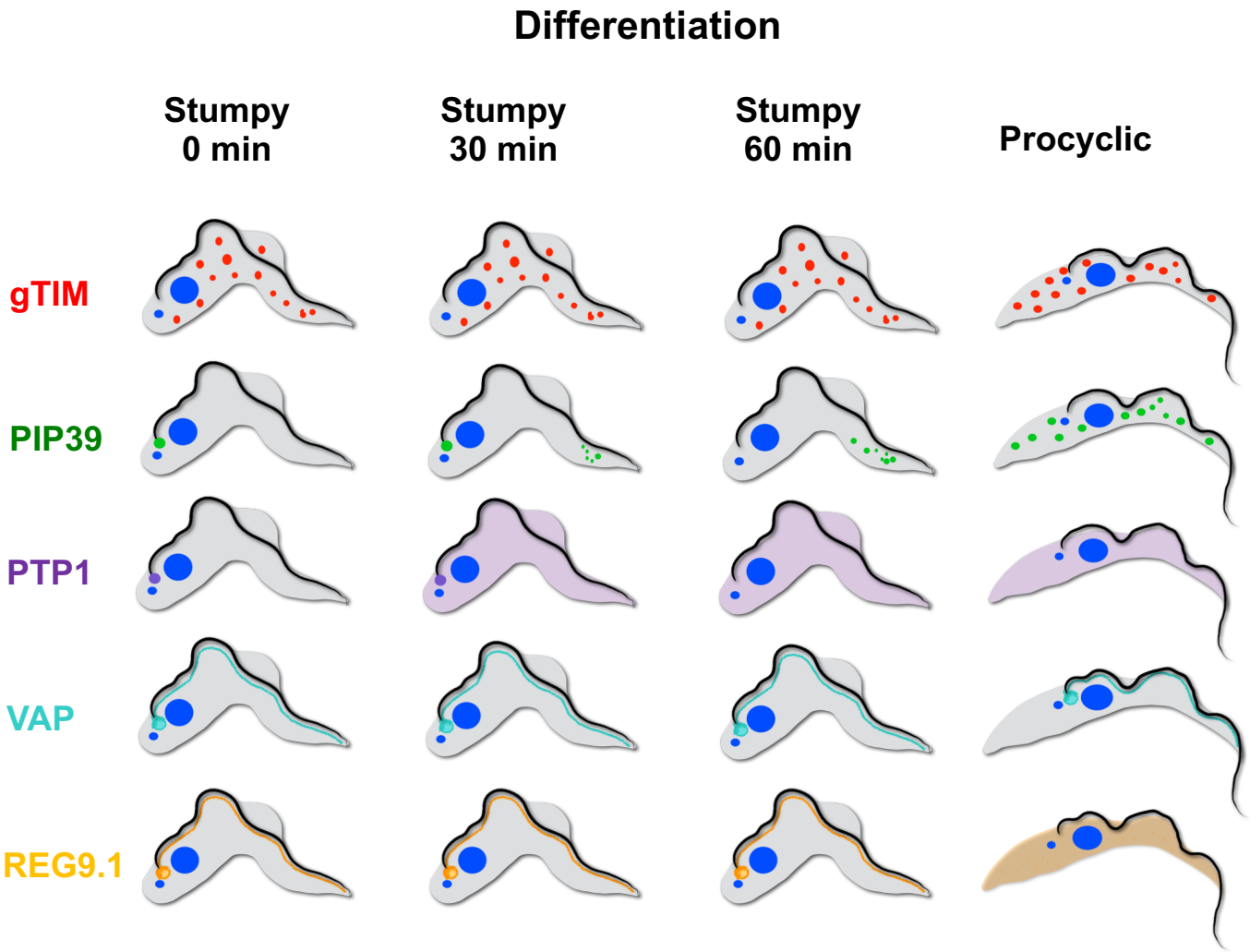
Differentiation
Stumpy
0 min
Stumpy
30 min
Stumpy
60 min
Procyclic
gTIM
PIP39
PTP1
VAP
REG9.1

Figure 9

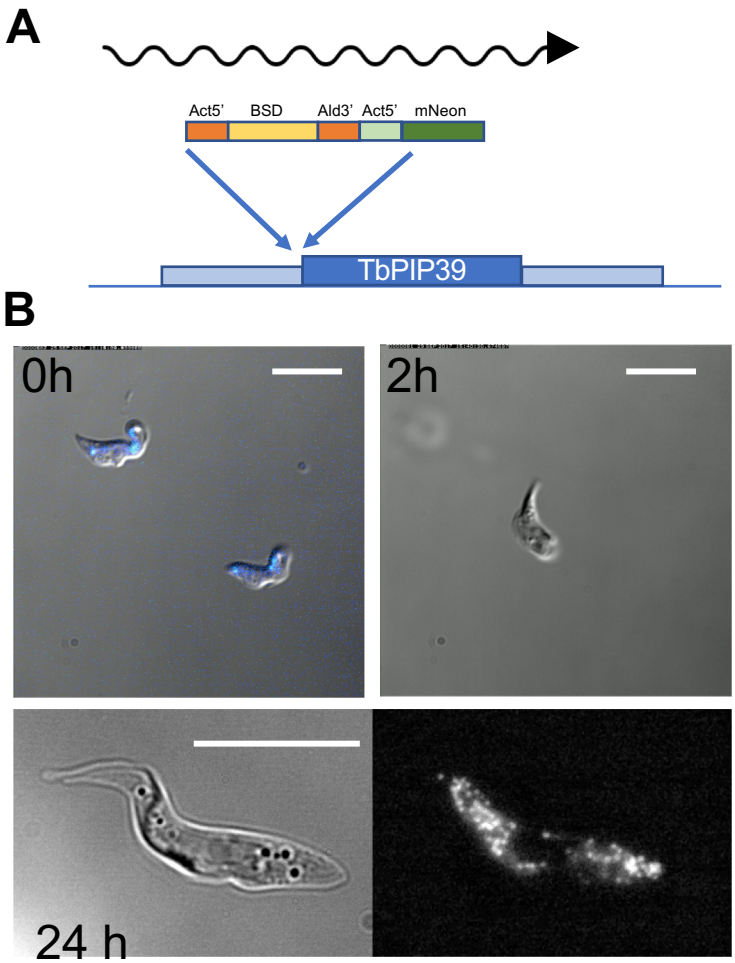

0h: movie S1A
2h: movie S1B
24h: movie S1C

Supplementary Figure 1

A

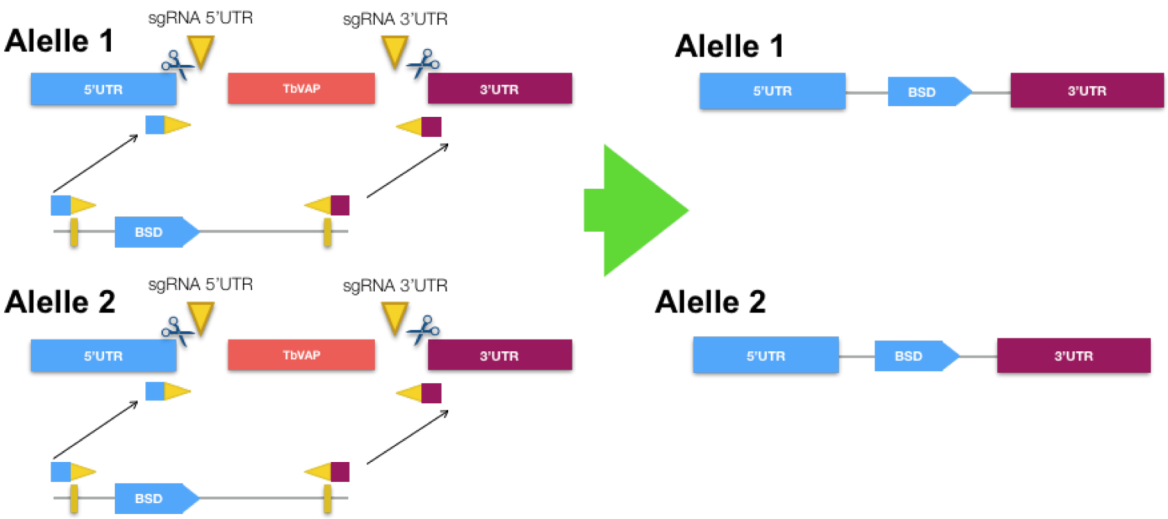

B

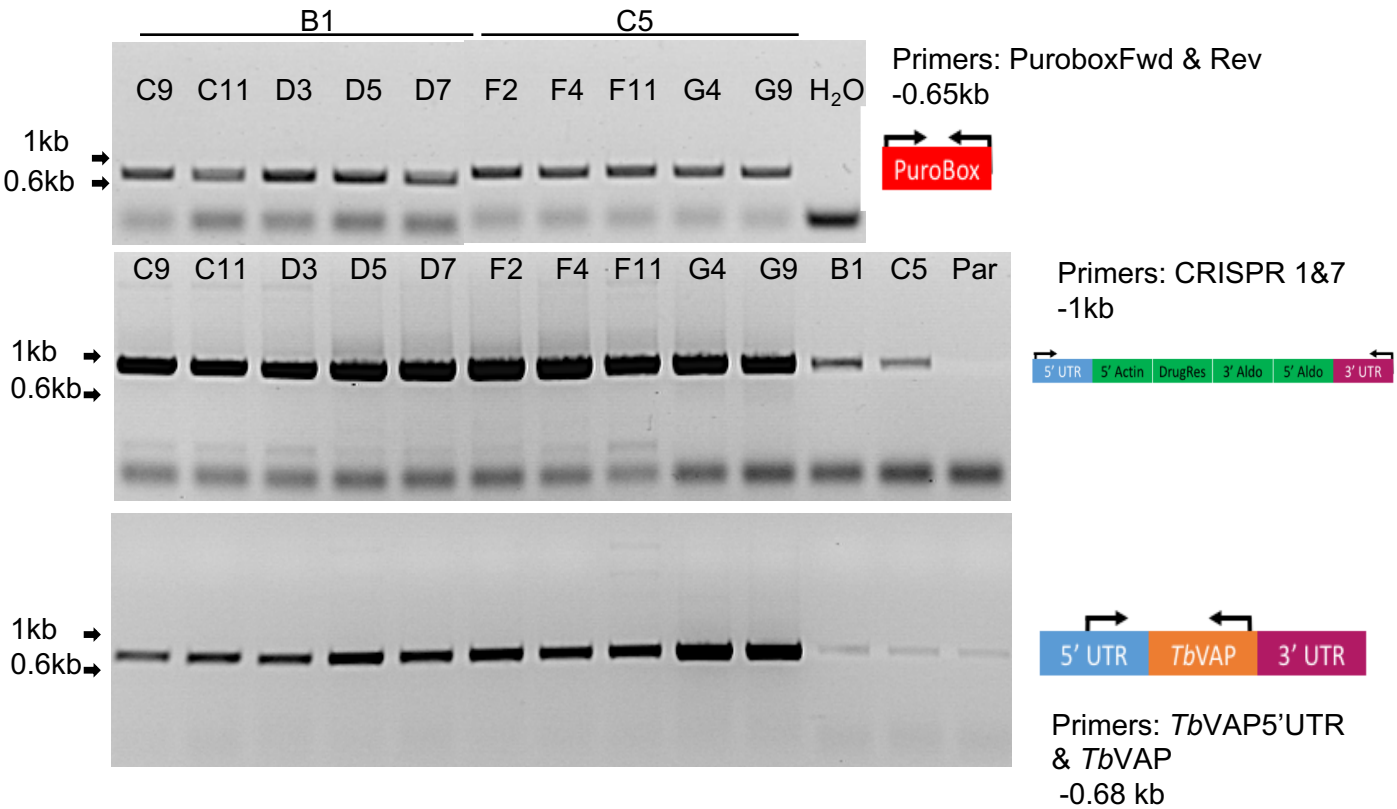

Supplementary Figure 2